Proceedings of the ASME 2011 International Mechanical Engineering Congress & Exposition
IMECE2011
November 11-17, 2011, Denver, Colorado, USA

IMECE2011-63918

MODELING OF SERRATED CHIP FORMATION WITH A FRACTURE LOCUS APPROACH

Yalla Abushawashi
Department of Mechanical Engineering
Michigan State University
Lansing, MI, USA

Xinran Xiao
Department of Mechanical Engineering
Michigan State University
Lansing, MI, USA

V. P. Astakhov
Production Service Management Inc. (PSMi)
Saline, MI, USA

ABSTRACT

A fracture model is of great concern when it comes to chip formation and simulation of localized shear bands that take place in serrated chip formation. Considering the special loading characteristics of the cutting regime, the present paper is intended to evaluate the equivalent fracture strain to be used in the prediction of segmented chip formation and energy evaluation. It is assumed that both the equivalent strain rate and stress triaxiality define the material fracture locus. The stress triaxiality analysis was based on the fracture experiments using flat-grooved specimen conducted by Bai et al. [1]. The effect of the strain rate was estimated based on the strain energy density and stress triaxiality. To ensure model completeness and solution stability, damage evolution was modeled based on the material fracture energy. Numerical simulations of machining AISI steel 1045 with and without friction model were performed. The physical and morphological characteristics of the chip formation were analyzed. The results were found to be in agreement with the experimental data of the actual segmented chip obtained from the literature. The anticipated fluctuation of the cutting force caused by the chip segmentation was observed. It is noted that up to 25% reduction of the total energy required by the system may be achieved by minimizing tool friction using tribological coating and/or metal working fluids.

INTRODUCTION

Metal cutting is one of the most common and oldest manufacturing operations with a wide range of today's cutting techniques such as turning, milling, drilling, grinding, etc. Understanding the process is the key to improve the efficiency and quality of the machined surfaces. Many researchers have performed analytical and experimental studies since the 19th century. Among them, Piispanen developed the card model in 1930s, Merchant introduced the orthogonal force model in 1945, and Oxley proposed the parallel sided shear zone theory in 1960. Most of the theories were based on simple observations of metal cutting which led to the development of the Single Shear Plane Model (SSPM) as known today. However, the SSPM and its idealized forms have shown a number of drawbacks. For example, Astakhov [2] concluded that the model lacks predictability and listed a number of critical issues with the SSPM, such as unrealistic material behavior, inapplicability for cutting brittle work materials, and misrepresentation of the tool-workpiece contact. The complex characteristics of the metal cutting process where the deformation takes place in a small volume under extremely intense condition were not well understood by the oversimplified analytical approaches and the need for numerical analysis is undisputable.

The development of Finite Element Method (FEM) in the early 1970s opened a new opportunity for the analysts to perform numerical investigations on metal cutting. Upon the vast use of the commercial software in 1990s and the advancement of the computational capabilities during the last two decades, enormous parametric studies for different work piece and tool materials were performed using numerical simulations [3-6]. Serrated chip formation simulations were among the topics which received considerable attention from the researchers. Depending on the material characteristics such

as the ductility and fracture toughness, chip segmentation often occurs in High Speed Machining (HSM) due to material strain rate sensitivity to fracture. Although many studies on the chip segmentation phenomenon have been published, only few addressed the prediction of both cutting force and chip morphology [5].

The success of any computational model using FEM is strongly dependent on the accurate characterization of the workpiece material, including the constitutive law and the fracture criteria. In particular, a fracture model is of extreme importance in modeling the shear bands resulting in formation of the saw-tooth shape of the chip. A complete fracture model should include a full description of the damage initiation and evolution. In ductile metals such as AISI steel 1045, damage initiation may be formulated based on the material ductility (equivalent strain at fracture $\bar{\varepsilon}_f$). Generally $\bar{\varepsilon}_f$ is sensitive to the state of stress (stress triaxiality and Lode angle) which in plane strain condition can be represented in terms of stress triaxiality only. To account for the HSM, strain rate sensitivity to fracture must be incorporated as well. In addition, FEM outcomes are greatly rely on the proper identification of the boundary conditions including friction and contact conditions. This paper addresses these concepts according to the following outlines.

- Calibration of the Johnson-Cook (JC) plastic flow model using literature data obtained from shear test [1].
- Explanation of the generalized 3D space of the fracture locus and its reduced plane strain space which is applicable for the loading condition particular for orthogonal cutting.
- Constructing the fracture locus based on the state of stress (stress triaxiality) at fracture using the numerical inverse approach and experimental fracture strain limit.
- Illustration of the strain rate sensitivity to fracture based on the strain energy density and stress triaxiality.
- Representation of material degradation beyond damage initiation.
- Workpiece-tool interface friction model.
- Finite element solution and chip separation mechanism.
- Results discussion and validation.

PLASTIC FLOW MODEL

Generally, the plastic flow of a material depends on its effective strain $(\bar{\varepsilon})$, strain rate $(\dot{\bar{\varepsilon}})$, and its temperature (T). It is often thus described as the product of these three functions as:

$$\bar{\sigma} = f\left(\bar{\varepsilon}\right) g\left(\dot{\bar{\varepsilon}}\right) h\left(T\right) \tag{1}$$

where $\bar{\sigma}$ is the effective stress.

The widely used the JC model [7] describes the material constitutive behavior in terms of the above three functions as:

$$\bar{\sigma} = \left[A + B\bar{\varepsilon}^{n} \right] \left[1 + C \ln\left(\frac{\dot{\bar{\varepsilon}}}{\dot{\bar{\varepsilon}}_o} \right) \right] \left[1 - \left(\frac{T - T_o}{T_m - T_o} \right)^{m} \right] \tag{2}$$

where A is the initial yield strength, B is the hardening modulus, and C is the strain rate sensitivity. These parameters and the hardening (n) and thermal softening (m) coefficients can be obtained by conducting material tests at low strain rates, various temperature levels by conventional tests, and at high strain rates using the Split Hopkinson Pressure Bar (SHPB) tests [7,8]. Parameters $\dot{\bar{\varepsilon}}_o$, T_o, and T_m in the JC model are the reference strain rate, the reference or room temperature, and the material melting temperature, respectively.

THERMAL SOFTENING IN MACHINING

Nearly all investigations on metal cutting have considered or at least mentioned the importance of the heat generation in machining process. In order to understand the implication of the temperature rise in the plastic flow behavior the sources of heat in the cutting system should first be identified.

Almost all the power consumed by the metal cutting system due to significant plastic deformation of the work materials and due to friction at the tribological interfaces is converted into heat [3,9]. As the cutting tool advances into the workpiece, the created chip undergoes a combined state of stresses in conjunction with a high strain rate which causes an instantaneous heat generation and local temperature rise. Specifically, in literature, the plastic deformation at the so-called shear plane in the primary zone has been considered as the main source of heat. A part of this energy is transmitted to the chip while the other propagates into the workpiece material. Heat is also generated due to friction along the chip-tool and workpiece-tool contact interfaces. Because a major portion of the energy spent in the cutting system is due to plastic deformation of the layer being removed, one may conclude that the thermal energy due to this deformation should be a major contributor into the total thermal energy in the machining system.

On the other hand, it is obvious that the mechanical tests for the characterization of the material flow parameters inherently involve large deformations. In such tests, the heat generation resulting from plastic energy is unavoidable. Moreover, the heat generated under high strain rate condition accelerates the temperature rise and creates adiabatic localized regions in both conventional experiments and machining alike. In other words, the strain rate hardening measured in high rate material testing may have included some thermal softening effects, similar to that observed in metal cutting. Therefore, presuming no external heat source added to the cutting system, the thermal softening function may be excluded from JC constitutive law and the yield surface in high speed machining may include only strain and strain rate terms, thus

$$\bar{\sigma} = \left[A + B\bar{\varepsilon}^{n} \right] \left[1 + C \ln\left(\frac{\dot{\bar{\varepsilon}}}{\dot{\bar{\varepsilon}}_o} \right) \right] \quad (3)$$

JOHNSON–COOK MODEL CALIBRATION

The shear test results [1] are used to obtain the effective yield surface hardening parameters under static loading condition. The least square optimization approach is applied to ensure the best mathematical representation of the experimental data. The JC model together with the equivalent stress-strain obtained from the tubular shear test is shown in Fig. 1. Table 1 contains the JC model parameters for AISI steel 1045.

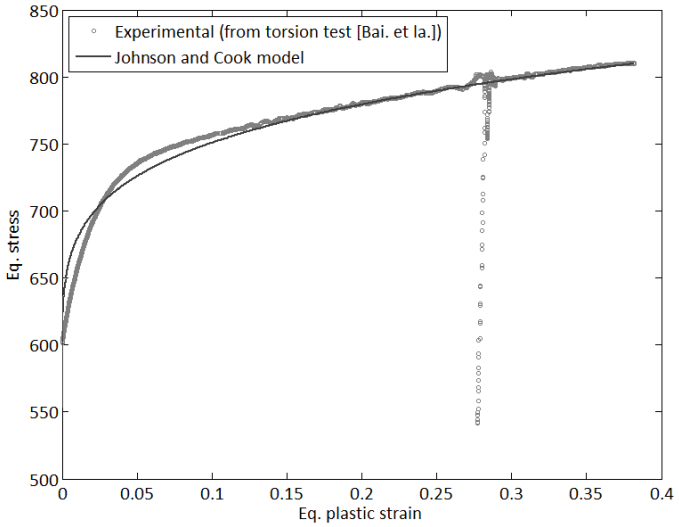

Fig. 1 JC equivalent plastic flow model optimization for AISI steel 1045 based on torsion test performed by Bai. et al. [1].

Table 1 Material constants used in simulation for AISI steel 1045.

Density and elasticity properties			
	Density (Kg/m^3)	Poisson's ratio	Young's modulus(MPa)
Work piece	7.8X10^3	0.3	2.2X10^5
Carbide tool	15X10^3	0.2	8.0X10^5
JC plasticity parameter [a]			
A (MPa)	*B (MPa)*	*C*	*n*
553.1	309.9	0.0134	0.1952
Fracture toughness properties ($MPa\sqrt{m}$)			
K_{IC}		K_{IIC}	
55.4		71.5	

[a] Parameters *A* and *C* are based on [10].

DUCTILE FRACTURE MODEL

Generally, metallic materials fail due to ductile fracture (based on initiation, growth and coalescence of voids) or shear fracture (based on shear band localization) [11]. Depending upon the stress state, failure could also occur through a process involving both mechanisms. Furthermore, fracture properties and damage behavior may change significantly within a single or across two different mechanisms.

The effective plastic strain limit is usually used to characterize the fracture of ductile materials. The strain at which damage is initiated typically depends on the loading condition. The stress triaxiality state reflects the mean stress (σ_m) which is equivalent to the spherical part of the stress tensor. It is defined by a dimensionless parameter $\eta = \sigma_m / \bar{\sigma}$ and is considered as an important factor in formulating ductile fracture models in the literature [1,11-14].

Rice and Tracey [15] studied the ductile growth and coalescences of microscopic voids under the superposition of hydrostatic stresses. They found that, for any remote strain rate field, the void enlargement rate is amplified over the remote strain rate by a factor rising exponentially with the triaxiality parameter according to the following function:

$$\bar{\varepsilon}_f = C_1 \mathrm{e}^{C_2 \eta} \quad (4)$$

where C_1 and C_2 are the material fracture constants to be determined experimentally, and $\bar{\varepsilon}_f$ is the corresponding equivalent fracture strain. Other researchers have developed similar relations. For instance, Johnson and Cook [8] introduced a fracture model which integrates the effect of stress triaxiality, strain rate, and temperature in a separable function with five independent material fracture constants.

Another parameter of the stress state, known as the normalized third deviatoric invariant, affects materials ductility, and thus affects the material fracture strain [13,14,16]. This parameter considers the influence of some combination of the deviatoric part of the stress tensor which is correspondent to the so-called Lode angle. The deviatoric state parameter is defined by the following equation:

$$\xi = \frac{27}{2} \frac{J_3}{\bar{\sigma}^3} \quad (5)$$

where J_3 is the third deviatoric invariant and ξ is the deviatoric state parameter $(-1 \le \xi \le 1)$.

Figure 2 shows a number of important spatial loading cases having significant practical meaning. The diagram can be viewed as a 2D projection of the 3D fracture surface. For example, it is possible to relate ξ and η by Eq. (6) in the case of plane stress state [12].

$$\xi = -\frac{27}{2} \eta \left(\eta^2 - \frac{1}{3} \right) \quad (6)$$

The tensile and compression axial symmetry loading states $\xi = 1$ and $\xi = -1$ can be achieved experimentally by using the classical notched or smooth round bar specimen. Also, the

equibiaxial tension and compression experiments lead to a similar state of stress [17].

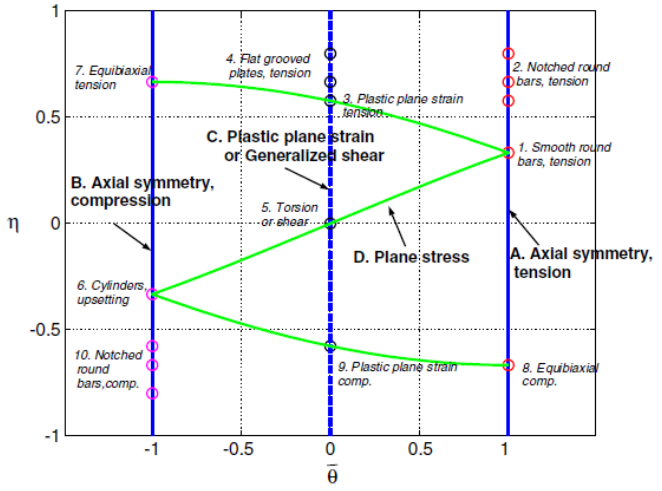

Fig. 2 Stress states diagram in the triaxiality and Lode angle parameter (equivalent to ξ) [17]

In the case of plane strain where the deviatoric parameter $\xi = 0$, the 2D fracture loci can be conveniently represented by an exponential relationship similar to Eq. (4) [17]. The plane strain fracture model may be calibrated using grooved plane strain specimen [1]. For calibration purposes, the pure shear torsion test may also be combined with other plastic plane strain experiments that are superimposed with the hydrostatic pressure to account for various triaxiality values. This can be accomplished by changing geometrical configuration of the flat test specimen (Fig. 3). The importance of this case is that the orthogonal machining is a process where the feed is usually much larger than the uncut chip thickness and the cutting direction is perpendicular to the cutting edge. These facts support the simplified 2D simulations and the validity of the plane strain analysis hypothesis in chip formation investigations.

CONSTRUCTING THE PLANE STRAIN FRACTURE LOCUS

As discussed in the previews section, the conventional orthogonal cutting generally maintains $\xi = 0$. This reveals that the ductility of the workpiece and chip materials is affected only by the triaxiality parameter. In order to construct a fracture model for such a process, the experimental setup should be designed focusing on the examination of fracture under similar loading conditions. For example, in addition to the zero deviatoric effect on the chip separation zone near tool tip, it is also under a positive stress triaxiality value because of the hydrostatic tensile stress originated before separation. On the other hand, the primary zone, where shear bands may be formulated under negative mean stress, may develop a negative triaxiality value.

Testing of a flat-grooved specimen can provide experimental data on the material fracture mechanics at regions of stress state where $\xi = 0$ that is different from those obtained with round-notched bars. Specimens of a circular bar shape provide information at the axial symmetry lines $\xi = \pm 1$ which is far away from the plane strain state existed in the conventional orthogonal metal cutting.

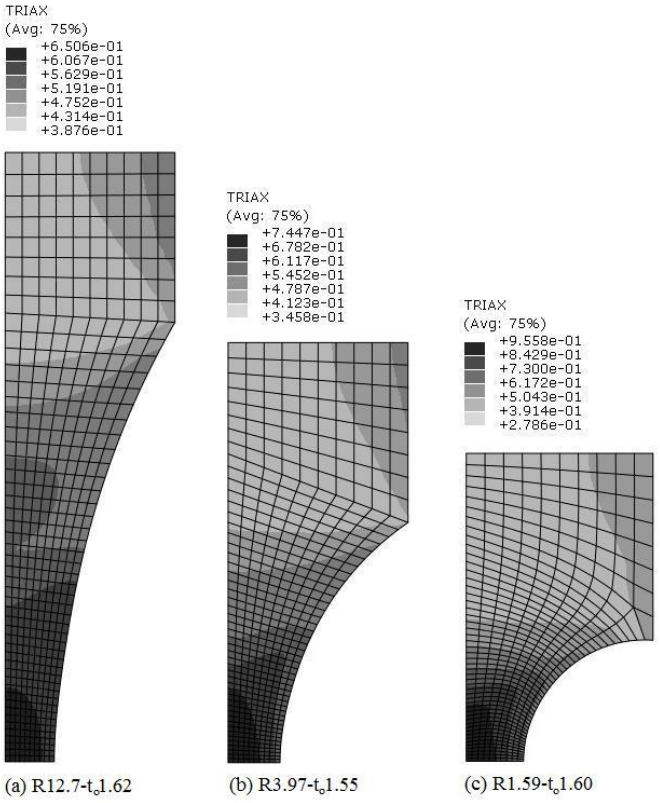

Fig. 3 Axis-symmetric finite element simulation with the stress triaxiality contours at fracture for three selected flat-grooved specimens made of AISI steel 1045. Specimen (a) groove radius *R=12.7mm*, ligament thickness t_o*=1.62mm*, specimen (b) *R=3.97mm*, to=1.55mm, and specimen (c) *R=1.59mm*, t_o*=1.60mm*

Bai et al. [1] have developed a stress triaxiality expression (Eq. (7)) for the flat grooved plate specemen. The formulation is similar to that of round notched bars developed by Bridgman in 1952. The developed relationship relates the triaxiality parameter to the ratio of the ligament thickness (t) and the radius of the groove (R). It is assumed that the material flow obeys a rigid-perfect-plastic law. In the authors' opinion the strain hardening existing in the elastic-plastic materials has a minor effect on the stress triaxiality parameter because the mean stress is normalized by the equivalent stress which reduces the triaxiality sensitivity.

$$\eta = \frac{\sqrt{3}}{3}\left[1 + 2\ln\left(1 + \frac{t}{4R}\right)\right] \quad (7)$$

In order to estimate the equivalent fracture strain $(\bar{\varepsilon}_f)$, the authors [1] used the following equation:

$$\bar{\varepsilon}_f = \frac{2}{\sqrt{3}}\ln\left(\frac{t_o}{t_f}\right) \quad (8)$$

The relation requires the specimen thickness at fracture (t_f) and the original specimen thickness (t_o) which can be measured directly. However, unless the material has a brittle-like rupture behavior, the necking may introduce practical difficulties in finding the exact onset fracture strain. As a result, the calculated $\bar{\varepsilon}_f$ may be overestimated and the obtained $\bar{\varepsilon}_f$ reflects the point where the material has lost all its stiffness.

The initial η calculated directly using Eq.(7) may differ from the final value at fracture. The triaxiality stress state development during plastic loading is restrained by the material constitutive law and the amount of plastic deformation during loading progression (Fig. 4). Therefore, it is expected to end up with a larger stress triaxiality value at fracture as compared to the initial value calculated by Eq. (7), which is estimated based on a perfect plasticity flow assumption.

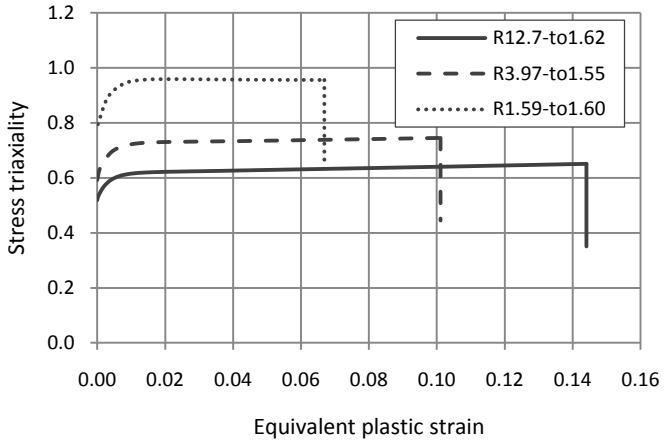

Fig. 4 Stress triaxiality evolution diagram of AISI steel 1045 obtained from finite element simulation for three selected flat-grooved specimens.

To account for the variation of stress triaxiality during loading, the average stress triaxiality value (η_{av}) instead of the initial value may be used. Knowing the required stress triaxiality history data, one can calculate η_{av} using the following equation:

$$\eta_{av} = \frac{1}{\bar{\varepsilon}_f}\int_0^{\bar{\varepsilon}_f} \eta(\bar{\varepsilon})\, d\bar{\varepsilon} \quad (9)$$

Wierzbicki et al. [1,18] performed parallel numerical simulations and used the triaxiality history output field with Eq. (9) to construct the fracture locus (Fig. 5). The authors used the measured displacement from experiments to indicate fracture in their finite element model. This approach can be used with a flat-grooved plate (or round-notched bar) specimen where η is expected to vary during experiments. However, the experimental results obtained from the pure shear test using a tubular specimen require no averaging because no axial loading is imposed $(\eta = \eta_{av} = 0)$.

Although the use of Eq. (9) indicates a complex contribution of the stress state path, it is still not clear whether stress state path $\left(\eta(\bar{\varepsilon})\text{ and }\xi(\bar{\varepsilon})\right)$ have an effect on the fracture locus and what the nature of its role is. However, the motivation of using Eq. (9) could be the consequence of uncertainty on the definition of the onset material fracture. Due to the evolution nature of fracture mechanics, the material loading capacity gradually degrades beyond the fracture initiation point but will not drop suddenly. Therefore, depending on the method of measurement, the measured displacement to fracture may not precisely indicate the fracture initiation. Furthermore, the prominent decrease in the specimen local cross-sectional area during necking results in localized large strains which severely affects the state of stress. These dramatic changes occurring during damage evolution may mislead the identification of the state of stress at fracture initiation.

Figure 5 shows a comparison of different approaches along with a similar work conducted here using the numerical analysis with the fracture strain limit calculated directly using Eq. (8). Fracture locus calculated by this method introduces much lower $\bar{\varepsilon}_f$ compared to the displacement limit model. However, the fracture locus suggested by Bai et al. [1], which uses η_{av} from simulation based on the displacement limit, did not include the tubular specimen results. Unlike flat-grooved specimen, a pure shear experiment does not have the complications of a changing triaxiality and therefore, should not be excluded.

It is assumed in this paper that under static loading condition, the followings are valid:

- The stress state is characterized by a stress triaxiality parameter at which a plane strain condition exists. This is motivated by the conventional mechanics of the orthogonal metal cutting.
- The fracture model of Rice and Tracey [15] is used to predict fracture under static loading condition and the superposition of hydrostatic stresses.
- Only the stress state at the onset of fracture may affect the stain limit under static loading condition. The stress state path has no influence on $\bar{\varepsilon}_f$.
- The damage evolution beyond the onset of fracture is of a brittle fracture type with a little or no degradation profile.

Table 2 shows the results of the stress triaxiality for the three different approaches including the final stress triaxiality (at fracture) approach. This model is used in the chip formation computational model. The two material damage parameters needed in Eq. (4) are found to be $C_1 = 0.465$ and $C_2 = -1.96$.

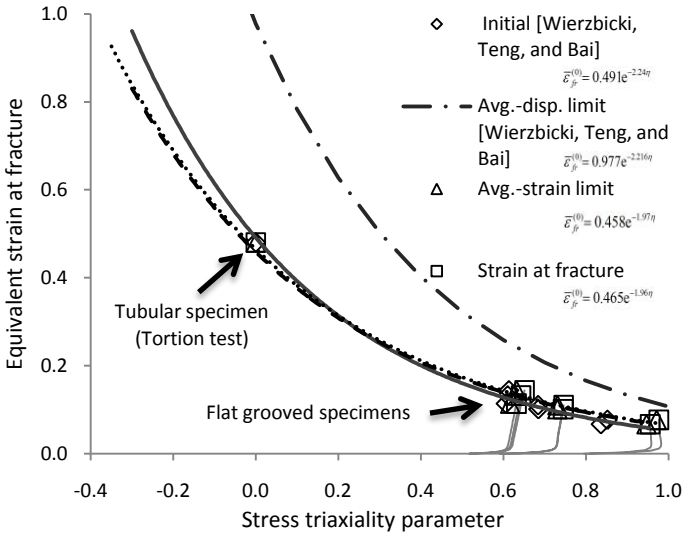

Fig. 5 AISI steel 1045 fracture locus based on initial stress triaxiality, averaged using displacement limit simulation model, averaged using strain limit model, and the fracture locus based on strain at fracture. Stress triaxiality evolution curves are also shown.

Table 2 The initial, final, and average stress triaxiality calculated using numerical simulation results for AISI steel 1045.

Experiment [a]	Stress triaxiality			Fracture strain [c]
	Initial [b]	At fracture	Average	
R12.7-to1.62	0.6136	0.6511	0.6319	0.1441
R12.7-to1.48	0.6105	0.6430	0.6256	0.1321
R12.7-to1.28	0.6061	0.6316	0.6166	0.1137
R3.97-to1.55	0.6849	0.7449	0.7310	0.1011
R3.97-to1.54	0.6842	0.7459	0.7312	0.1101
R1.59-to1.60	0.8365	0.9557	0.9471	0.0669
R1.59-to1.71	0.8523	0.9767	0.9717	0.0768
Tubular-torsion	0.0000	0.0000	0.0000	0.4787

[a] For detailed experimental data refer to [1].
[b] Calculated directly from Eq. (7).
[c] Calculated directly from Eq. (8). For tubular specimen refer to [1].

Therefore:

$$\bar{\varepsilon}_{fr}^{(0)} = 0.465e^{-1.96\eta} \tag{10}$$

In Eq.(10), the superscript in $\bar{\varepsilon}_{fr}^{(0)}$ indicates the plane strain condition and the subscript indicates fracture at the reference strain rate.

THE INDIRECT EFFECT OF STRAIN RATE ON FRACTURE

High-speed machining (HSM) helps manufacturers to improve machining efficiency [19]. HSM has many advantages over the conventional machining such as improving the quality of the machined surface and reducing cost. In addition to the high material removal rate, it is observed that the cutting speed reduces the cutting force and increases tool life [5,20]. Due to these economical and technical advantages, HSM technology has become very popular in many industries. HSM, however, introduces new scientific challenges. Unlike the conventional machining, HSM develops elevated strain rates ranging from 10^3 to 10^6 s^{-1} [21]. Generally, strain rates can be classified into three regions which are ranging from low $(\dot{\bar{\varepsilon}} < 1)$ to high $(\dot{\bar{\varepsilon}} > 10^3)$. HSM strain rates are considered to be high and the influence of the equivalent strain rate $(\dot{\bar{\varepsilon}})$ can be substantial [20].

Many fracture models considered a strain rate factor in their formulations. , including the JC model [8]. However, the JC damage model does not include all stress state parameters. Even with the separable nature of the proposed model and its availability in most commercial FE packages such as ABAQUS© and LS-DYNA©, it remains unclear how the five material fracture constants are calibrated. Recently, Leppin et al. [11] succefully predicted the results of dynamic axial crash test using numerical simulation. The fracture model treats the ductile and shear fracture modes separately and introduces the ductile and shear equivalent plastic strains $(\bar{\varepsilon}_{fd}, \bar{\varepsilon}_{fs})$, both of which are functions of the strain rate. It was assumed that fracture occurs when one of these equivalent plastic strain accomulations reaches a critical value.

In the context of the current development, the generalized equivalent plastic strain fracture model introduced by Clift et al. [22] can be considered. It is postulated that fracture occurs when the equivalent pastic strain weighted by the equivalent stress $(\bar{\sigma})$

$$E = \int_0^{\bar{\varepsilon}_f} \bar{\sigma} d\bar{\varepsilon} \tag{11}$$

achieves a predefined critical value E.

Note that Eq.(11) has a unit of energy density. The model suggests that the material toughness is a constant value and the area underneath the stress strain curve does not change. However, since the equivalent strain at fracture in general is a function of stress state, it can be concluded that the critical value E cannot be independent from stress state. Specifically, for every state of stress at fracture (η_f, ξ_f), there will be a different E value. Therefore, Eq. (11) may be rewritten as:

$$E\left(\textit{stress state at fracture}\right)=\int_0^{\bar{\varepsilon}_f}\bar{\sigma}d\bar{\varepsilon} \tag{12}$$

Although Eq. (12) contains the equivalent stress which depends on the strain rate according to Eq. (1), the total amount of specific energy to fracture E is independent of strain rate. However, the equivalent strain at fracture $(\bar{\varepsilon}_f)$ will still depend on the strain rate because of the material strain rate hardening.

For an adiabatic loading condition where no heat flows from the surrounding to the system, the substitution of Eq. (1) into Eq. (12) yields:

$$E\left(\xi_f,\eta_f\right)=\int_0^{\bar{\varepsilon}_f} f\left(\bar{\varepsilon}\right)g\left(\dot{\bar{\varepsilon}}\right)d\bar{\varepsilon} \tag{13}$$

For a separable strain fracture model that depends on both stress state at fracture and strain rate, the general equivalent strain at fracture is introduced in the following form

$$\bar{\varepsilon}_f(\xi_f,\eta_f,\dot{\bar{\varepsilon}})=S(\xi_f,\eta_f)R(\dot{\bar{\varepsilon}}) \tag{14}$$

where S is the fracture locus at the reference equivalent strain rate $\dot{\bar{\varepsilon}}_o$, and R is the fracture strain rate sensitivity function. Considering the special case where $\dot{\bar{\varepsilon}}$ is a constant during plastic deformation and all the way to the fracture, the integration and separation of Eqs. (13) and (14) provides the following result

$$R(\dot{\bar{\varepsilon}})=\left[g(\dot{\bar{\varepsilon}})\right]^{-2/(n+2)} \tag{15}$$

Note that, for the case of plane strain loading, the reference fracture locus S depends only on the stress triaxiality at fracture as described by Eq. (4). The overall equivalent plastic strain at fracture can be obtained by combining Eqs. (14) and (15) as:

$$\bar{\varepsilon}_f(\xi_f,\eta_f,\dot{\bar{\varepsilon}})=S(\xi_f,\eta_f)\left[g(\dot{\bar{\varepsilon}})\right]^{-2/(n+2)} \tag{16}$$

Using the JC strain rate function term $g(\dot{\bar{\varepsilon}})$ from Eq. (3) and the reference fracture locus $(S=\bar{\varepsilon}_{fr}^{(0)})$ from Eq. (4), the following plane strain fracture model can be obtained:

$$\bar{\varepsilon}_f^{(0)}(\eta_f,\dot{\bar{\varepsilon}})=C_1e^{C_2\eta_f}\left[1+C\ln\left(\frac{\dot{\bar{\varepsilon}}}{\dot{\bar{\varepsilon}}_0}\right)\right]^{-2/(n+2)} \tag{17}$$

This result governs the material ductile fracture which obeys the JC constitutive law and uses material flow sensitivity to the strain rate to account for the fracture strain rate sensitivity. Equation (16) represents a special case where the loading process maintains a constant $\dot{\bar{\varepsilon}}$. To account for the strain rate path that is not constant and/or using a different constitutive model, Eq. (13) should be used. Figure 6 shows the stress triaxiality contours in the $\bar{\varepsilon}_f^{(0)}$ and $\dot{\bar{\varepsilon}}$ space for AISI steel 1045. The curves indicate material ductility declination with the increase of the strain rate. Another observation is that for the conditions at low and negative stress triaxiality, similar to the conventional metal cutting, it is expected that $\bar{\varepsilon}_f^{(0)}$ will drop significantly with increasing the rate compared to higher values of stress triaxiality.

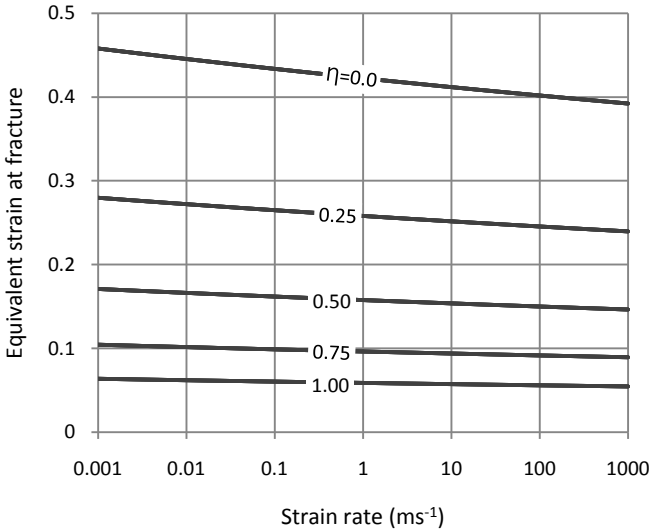

Fig. 6 The strain rate impact on the equivalent fracture strain at different stress states for AISI steel 1045.

DAMAGE EVOLUTION AND POST FAILURE CONTRIBUTION

Ductile fracture before final failure goes through extreme plastic deformation and damage evolution. Specimens in a uniaxial tensile stress test at some point start to develop microscopic voids in a process called void formation and coalescence. Those growing voids initiate micro-cracks in a progressive way which eventually leads to failure. The damage initiation site may be different from the observed fracture site. Figure 7 shows a hypothetic undamaged stress strain curve along with the one obtained from a conventional uniaxial stress test. The elastic-plastic undamaged path abc is followed by the departure of the experimental yield surface from the virtual undamaged yield surface at point c. Point c can be considered as the hypothetic damage initiation site where the material hardening modulus becomes progressively sensitive to the amount of damage leading to the declination of the material loading capacity. The hypothetic damage initiation site c also marks the start of elasticity modulus degradation. Due to increased damage, the material reaches its ultimate stress state and the hardening modulus becomes zero. This usually occurs in ductile metals when the material loading capacity decreases by 30% to 70% of its full capacity due to the accumulated damage [6]. The observed fracture initiation site is denoted by point e and finally the theoretical failure is indicated by point f.

To estimate the material stiffness degradation after damage initiation at point c, material fracture energy (G_f) introduced by Hillerborg et al. [23] may be used. Hillerborg postulated that the energy dissipated during material degradation process is

characterized by the amount of energy required to open a unit area of crack. This energy is a material property which can be calculated for the plane strain condition as:

$$G_f = \frac{1-\nu^2}{E} K_c^2 \tag{18}$$

where ν is the Poisson's ratio, E is the Young's modulus, and K_c is the material fracture toughness which depends on the damage mechanism. K_c is replaced by the fracture toughness of crack opening mode (K_{Ic}) when used for the separation zone (sacrificed elements), and replaced by the shear mode fracture toughness (K_{IIc}) when used to model the chip formation zone. The scalar damage parameter D is assumed to grow exponentially according to the following equation:

$$D = 1 - \exp\left(\frac{1}{G_f} \int_{\bar{\varepsilon}_c^p}^{\bar{\varepsilon}_f^p} L\bar{\sigma} d\bar{\varepsilon}^p \right) = 1 - \exp\left(\frac{1}{G_f} \int_0^{\bar{u}^p} \bar{\sigma} d\bar{u}^p \right) \tag{19}$$

where $\bar{\varepsilon}_c^p$ *and* $\bar{\varepsilon}_f^p$ are the equivalent plastic strains at points c and f in Fig. 7.

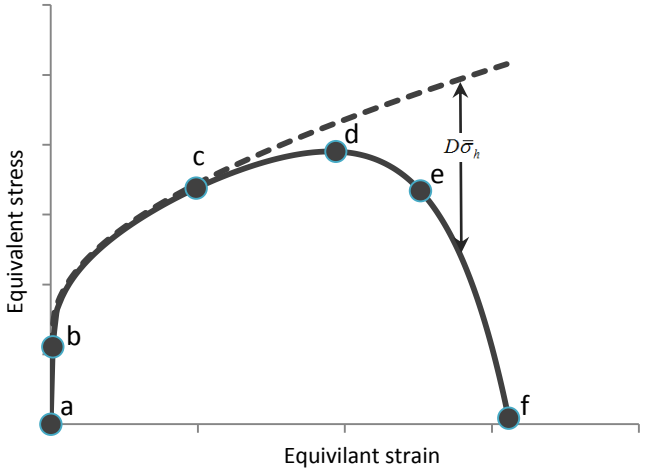

Fig. 7 Typical metal stress strain response in a uniaxial test.

It is critical to use the equivalent plastic displacement $(\bar{u}^p)$ instead of the equivalent plastic strain $(\bar{\varepsilon}^p)$ in finite element simulations. Beyond damage initiation, the material exhibits a strain softening behavior which leads to strain localization and a strong mesh dependency. To reduce this dependency the element characteristic length (L) is used to formulate stress-displacement relations. The material is assumed to start the strain softening and degradation process when the damage indicator (ω)

$$\omega = \sum_{j=1}^{m} \frac{\Delta\bar{\varepsilon}^p}{\bar{\varepsilon}_c^p} \tag{20}$$

reaches unity. In this equation, m is the total number of loading increments and $\Delta\bar{\varepsilon}^p$ is the equivalent plastic strain increase during the loading increment j.

The scalar damage parameter (D) is used to describe the material flow past damage initiation by the following relationship:

$$\bar{\sigma} = (1-D)\bar{\sigma}_h \tag{21}$$

where $\bar{\sigma}_h$ is the hypothetic undamaged stress estimated by Eq.(3).

TOOL-CHIP INTERFACE FRICTION MODEL

Due to severe normal stress at the tool-chip interface, the conventional proportional friction theory, the so-called Coulomb friction model, may result in shear traction that exceeds the chip ultimate shear strength (Astakhov [24]). This usually occurs within the contact length (l_c) near cutting edge where the normal stress is high. To overcome this violation, a sticking-sliding contact model is usually implemented. The model limits the maximum shear stress to a prescribed value over the sticking zone. In order to identify a friction model that is valid for metal cutting simulations, Rech et al. [25] performed the pin-on-ring system analysis and used the tribometer to extract experimental data such as sliding velocity and pressure. The study was made for annealed AISI steel 1045 with TiN coated carbide tools for the sliding velocities ranging from 75 to 150m/min. It was assumed that the total friction coefficient is due to the effect of two phenomena: the ploughing and the adhesive phenomenon. It is understood that for metal cutting simulations only the adhesive type of friction must be supplied. To isolate the ploughing effects, the authors conducted a thermo-mechanical numerical analysis to estimate the two quantities separately. The analysis is based on the comparison of the friction and heat flux with the experimental data obtained under similar condition. The final adhesive friction coefficient (μ_{adh}) model

$$\mu_{adh} = 0.498 - 0.002 \cdot V_{ls} \tag{22}$$

was found to be very sensitive to the average local sliding velocity (V_{ls}) which is ranging from 50 to 103 m/min.

FINITE ELEMENT SOLUTION

A commercial FEA software, ABAQUS© explicit, is used in the present paper to simulate the orthogonal metal cutting process with the segmented chip formation. The above constitutive and damage approaches are applied correspondingly to the elements for the workpiece. The sacrificing elements, which represent the separation zone, have been assigned a fracture energy calculated using K_{Ic} instead of K_{IIc}. The carbide cutting tool is assumed to have a sharp edge and modeled according to linear elasticity with the material parameters described in Table 1. The workpiece and the cutting tool were meshed using the 2D

continuum bilinear plane strain quadrilateral elements CPE4RT with reduced integration. The undeformed mesh and the prescribed boundary condition are shown in Fig. 8.

Due to the expected large deformations, localized strains, and shear bands in the serrated chip formation, element distortions is of great concern and should be handled carefully. To ensure structural distribution, the elements in the sacrificing zone and in the uncut chip layer were seeded with high element density. The element size was minimized in these regions to increase the accuracy and ensure the forming of the actual chip morphology. The workpiece was fixed at the bottom side and all other edges were allowed to deform without restraints. The tool was moving in the cutting direction by controlling the velocity of the back side of the tool to allow tool deformation.

CHIP SEPARATION MECHANISM

According to the damage initiation model described in this paper, the elements under hydrostatic pressure start their post damage degradation behavior at considerably higher equivalent strains compared with the ones under a low or negative pressure state. Beyond damage initiation, the degradation evolution suggested by Eq. (19) dictates that the material will lose all its loading carrying capacity (100% degradation) at a virtually infinite equivalent strain. The advantage of this model is that all elements including the severely damaged ones will still carry hydrostatic pressure and represent a fluid like contribution. The downside is the inability to simulate crack propagation and separation phenomena. To simulate a crack requires a separation mechanism.

The separation mechanism used in this work is based on the elimination of the "fully" damaged elements. Obviously, "fully" degradation does not exist with the application of the present exponential model. To overcome this difficulty, the elements with a positive triaxiality are deleted when reaching a degradation of 99% or greater. Those elements will be eliminated from the further analysis in the subsequent time increments. Although this separation mechanism is simple and computationally effective, this natural choice unavoidably creates hypothetic voids and develops new system conditions which may lead to solution instability issue if not handled properly.

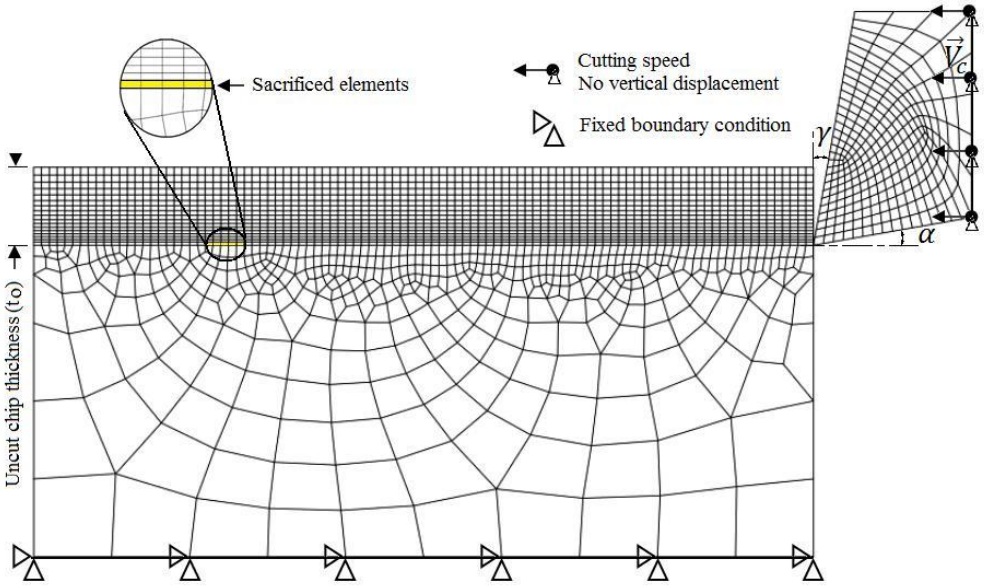

Fig. 8 Finite element model: the undeformed mesh and the prescribed boundary condition.

FINITE ELEMENT RESULTS AND DISCUSSION

Numerical simulations of segmented chip formation were carried out using the machining parameters shown in Table 3. The uncommonly large scale of the uncut chip thickness used in this study is intentionally proposed to avoid mass scaling issues and minimize the effect of the impractical tool edge roundness. The aim here is to look at the overall picture of the serrated chip characteristics rather than a specific machining condition. To understand the penalty of the contact interface, a frictionless model is also analyzed and compared with the full model.

The total cutting force shown in Fig. 11 reveals the cyclic nature of the chip formation that is in line with the definition of the metal cutting process proposed by Astakhov [26]. The number of the rises and falls is equal to the number of the produced segments in both cases. In the same time span (about 0.3 ms) the frictionless model produced 10 segments while only 7 were formed by the full model. Both the fluctuation magnitude and the average value are different and tend to be higher in the full model. In this particular case the average cutting force was increased significantly by about 25%.

In Fig. 9, obviously the degree of the chip curl is connected to the amount of the sliding resistance. The simulations imply that, for HSM where the friction coefficient is reduced (according to Eq.(22)), the chip tends to bend. Figure 9 shows

the damage indicator ω calculated based on the accumulated equivalent plastic strain. Shear bands with partially and fully damaged elements are responsible for the creation of the serrated chip morphology. Although the cutting process is different (geometrical magnification factor is 10), a qualitative morphological comparison with the actual chip (Fig. 10) as well as some dimensionless quantitative measurements demonstrate similarity in the overall shape of the produced segments.

Table 3 Cutting condition used in the simulation.

Cutting speed, V_o (m/min)	300
Uncut chip thickness, t_o (mm)	2
Depth of cut, d (mm)	10
Rack angle, γ (deg.)	10
Tool clearance angle, α (deg.)	10
Tool edge roundness	Sharp

The simulated chip with the interface friction has almost a straight shape similar to the actual chip. The predicted shear bands direction has similar characteristics but is not exactly parallel to that was measured in experiments. The predicted shear angle is about 27.2^o while the actual angle is 31^o. The average peak/valley ratio was calculated using the nodal coordinates (h_1/h_2=1.46) and compared with the experimental measurements (1.41). The Chip Compression Ratio (CCR) can also be estimated using the peak distance as an equivalent chip thickness. The calculated CCR from the finite element model was 1.40 and the measured CCR was 1.43. Although this dimensionless analysis of the chip morphology shows a good estimation of the proposed model, further investigations on the validity of such approach are necessary [27].

CONCLUSIONS

Simulations of metal cutting in general and serrated chip formation in particular are highly sensitive to the choice of a particular fracture model. The proposed progressive damage approach was found to be suitable when all loading conditions of the cutting process are considered. The stress triaxiality was estimated using the shear test results and the flat-grooved specimen under a uniaxial tensile load. Further experiments may be needed to avoid the extrapolation on estimating the fracture strains at negative triaxiality.

According to the proposed energy approach, the fracture locus sensitivity to the strain rate can be conveniently formulated based on a material constitutive law. It was found that, for the case of AISI steel 1045 as the work material, the strain rate is more significant to the material ductility in the lower and negative stress triaxiality; the conditions under which metal cutting occurs. A considerable reduction on the fracture strain was observed in the range of 10^{-3} to 10^{3} ms^{-1}. In metal cutting applications, it is recommended that the post damage material behavior should be integrated with the material fracture model. The fracture energy model with an exponential damage evolution ensures smooth material degradation and enhances computational stability.

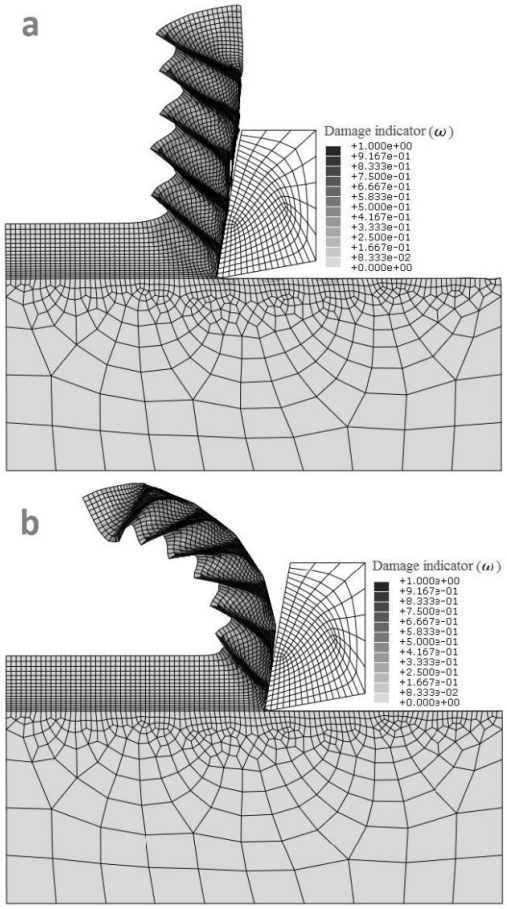

Fig. 9 Finite element simulation of the serrated chip formation with: (a) Contact friction, and (b) no friction at the tool-chip interface.

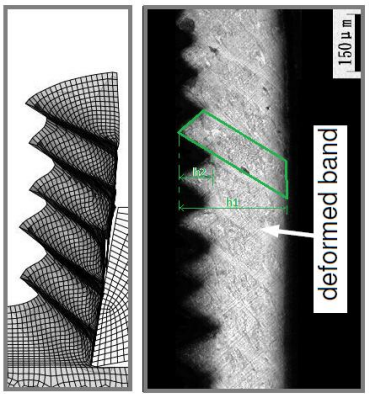

Fig. 10 Comparison between the experimental and modeled segmented chip morphology. Ref. [28] *(cutting speed V_c=432.6m/min, uncut chip thickness t_o=0.2mm, and rake angle $\gamma = 10^o$)*

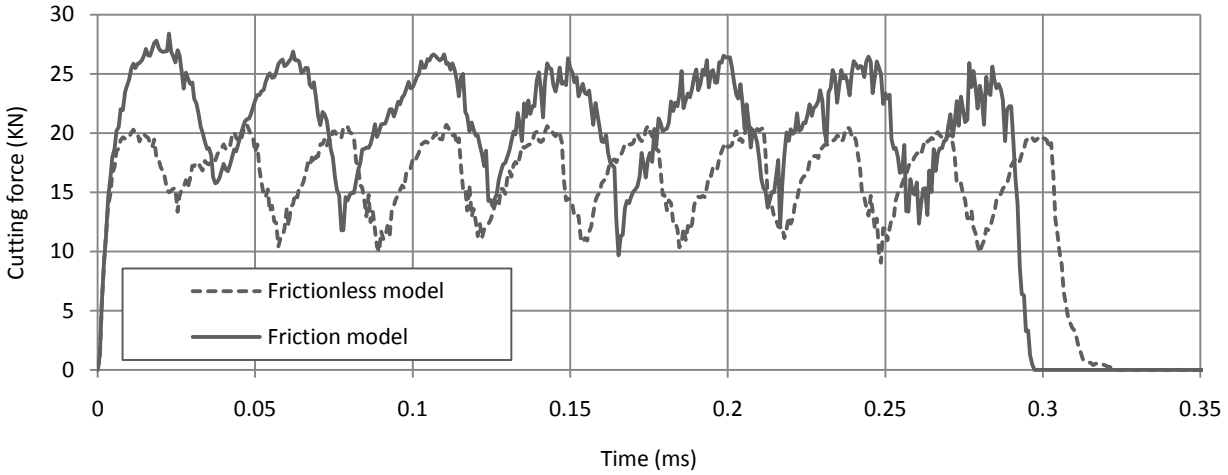

Fig. 11 Curves of the cutting forces for machining AISI steel 1045 with and without accounting for tool-chip interface friction.

The orthogonal metal cutting process was idealized using 2D plane strain finite elements. FE analysis successfully predicted the serrated chip and the formation of the shear bands. Dimensionless quantities describing the chip geometry such as shear band angle, CCR, and peak/valley ratio, were compared with the actual chip to evaluate the validity of the proposed fracture approach. The results were found to be very similar with a maximum error in the shear band angle of 2.9^o less than the actual value of 31^o. Unsurprisingly, the cutting force curves were fluctuating in a periodic way following the formation of the segments. The obtained cutting force and chip curl were also compared with the simulation of the serrated chip formation under frictionless contact conditions. The frictionless cutting operation under the present machining parameters consumes about 25% less energy than the actual full model.

The results significant for practical optimization of machining operations are:

1. Stress triaxiality significantly affects the fracture strain, and consequently the energy required for plastic deformation of the layer being removed is also affected. This observation is significant because: (a) the energy associated with this deformation constitutes up to 70% of the total energy required by the cutting system for its existence [29], and (b) this plastic deformation is nuisance of metal cutting so that the associated energy is a total waste [30], the reduction of this energy by adjusting stress triaxiality is the major reserve in increasing efficiency of the cutting process. This adjustment can be made by the tool geometry parameters.
2. The reduction of friction at the tool chip interface in HSM and in machining of difficult-to-machine materials (in both cases, the serrated chip is produces) by using tribological coating and/or metal working fluids of high lubricity can significantly improve chip breakability [31] as chip curvature increases. In other words, chip breakability improves with the reduction of friction at the tool-chip interface.

ACKNOWLEDGEMENT

The authors gratefully acknowledge the experimental data provided by Prof. Yuanli Bai.

REFERENCES

[1] Bai, Y., Teng, X., and Wierzbicki, T., 2009,"On the application of stress triaxiality formula for plane strain fracture testing," *Journal of Engineering Materials and Technology*, vol. 131, p. 021002.

[2] Astakhov, V.P., 2005,"On the inadequacy of the single-shear plane model of chip formation," *International Journal of Mechanical Sciences*, vol. 47, pp. 1649-1672.

[3] Majumdar, P., Jayaramachandran, R., and Ganesan, S., 2005,"Finite element analysis of temperature rise in metal cutting processes," *Applied Thermal Engineering*, vol. 25, no. 1359-4311, pp. 2152-2168.

[4] Duan, C.Z., Dou, T., Cai, Y.J., and Li, Y.Y., 2009,"Finite Element Simulation and Experiment of Chip Formation Process during High Speed Machining of AISI 1045 Hardened Steel," *International Journal of Recent Trends in Engineering*, vol. 1, pp. 46-50.

[5] Umbrello, D., 2008,"Finite element simulation of conventional and high speed machining of Ti6Al4V alloy," *Journal of Materials Processing Technology*, vol. 196, no. 0924-0136, pp. 79-87.

[6] Zhang, Y.C., Mabrouki, T., Nelias, D., and Gong, Y.D., 2011,"Chip formation in orthogonal cutting considering interface limiting shear stress and damage evolution based on fracture energy approach," *Finite Elements in Analysis and Design*, vol. 47, pp. 860-863.

[7] Johnson, G.R. and Cook, W.H., 1983,"A constitutive model and data for metals subjected to large strains, high strain rates and high temperatures," in *Proceedings of the*

7th International Symposium on Ballistics, vol. 21, Netherlands, pp. 541-547.

[8] Johnson, G.R. and Cook, W.H., 1985,"Fracture characteristics of three metals subjected to various strains, strain rates, temperatures and pressures," *Engineering Fracture Mechanics*, vol. 21, no. 0013-7944, pp. 31-48.

[9] Abukhshim, N.A., Mativenga, P.T., and Sheikh, M.A., 2006,"Heat generation and temperature prediction in metal cutting: A review and implications for high speed machining," *International Journal of Machine Tools and Manufacture*, vol. 46, no. 0890-6955, pp. 782-800.

[10] Jaspers, S. and Dautzenberg, J.H., 2002,"Material behaviour in conditions similar to metal cutting: flow stress in the primary shear zone," *Journal of Materials Processing Technology*, vol. 122, pp. 322-330.

[11] Leppin, C., Hooputra, H., Werner, H., Weyer, S., and Buchi, R.V., 2005,"Crashworthiness simulation of aluminium pressure die castings including fracture prediction," in *VIII International Conference on Computational Plasticity*, Barcelona, pp. 5-8.

[12] Wierzbicki, T. and Xue, L., 2005,"On the effect of the third invariant of the stress deviator on ductile fracture," Massachusetts Institute of Technology, Cambridge, MA, Lab report 136,.

[13] Teng, X. and Wierzbicki, T., 2006,"Evaluation of six fracture models in high velocity perforation," *Engineering Fracture Mechanics*, vol. 73, pp. 1653-1678.

[14] Wierzbicki, T., Bao, Y., Lee, Y.W., and Bai, Y., 2005,"Calibration and evaluation of seven fracture models," *International Journal of Mechanical Sciences*, vol. 47, no. 0020-7403, pp. 719-743.

[15] Rice, J.R. and Tracey, D.M., 1969,"On the ductile enlargement of voids in triaxial stress fields," vol. 17, no. 0022-5096, pp. 201-217.

[16] Xue, L., 2007,"Damage accumulation and fracture initiation in uncracked ductile solids subject to triaxial loading," *International Journal of Solids and Structures*, vol. 44, no. 0020-7683, pp. 5163-5181.

[17] Bai, Y. and Wierzbicki, T., 2008,"A new model of metal plasticity and fracture with pressure and Lode dependence," *International Journal of Plasticity*, vol. 24, no. 0749-6419, pp. 1071-1096.

[18] Bao, Y. and Wierzbicki, T., 2004,"On fracture locus in the equivalent strain and stress triaxiality space," *International Journal of Mechanical Sciences*, vol. 46, no. 0020-7403, pp. 81-98.

[19] Velasquez, J., Bolle, B., Chevrier, P., Geandier, G., and Tidu, A., 2007,"Metallurgical study on chips obtained by high speed machining of a Ti–6 wt.%Al–4 wt.%V alloy," in *Mate Sci Eng A*, pp. 452-453.

[20] Davim, J.P. and Maranhao, C., 2009,"A study of plastic strain and plastic strain rate in machining of steel AISI 1045 using FEM analysis," *Materials & Design*, vol. 30, no. 0261-3069, pp. 160-165.

[21] Jaspers, S. and Dautzenberg, J.H., 2002,"Material behaviour in metal cutting: strains, strain rates and temperatures in chip formation," *Journal of Materials Processing Technology*, vol. 121, no. 0924-0136, pp. 123-135.

[22] Clift, S.E., Hartley, P., Sturgess, C.E.N., and Rowe, G.W., 1990,"Fracture prediction in plastic deformation processes," *International Journal of Mechanical Sciences*, vol. 32, pp. 1-17.

[23] Hillerborg, A., Modeer, M., and Petersson, P.E., 1976,"Analysis of crack formation and crack growth in concrete by means of fracture mechanics and finite elements," *Cement and concrete research*, vol. 6, pp. 773-781.

[24] Astakhov, V.P., 2006,*Tribology of Metal Cutting*. London: Elsevier, vol. 52.

[25] Rech, J., Claudin, C., and D'Eramo, E., 2009,"Identification of a friction model-Application to the context of dry cutting of an AISI 1045 annealed steel with a TiN-coated carbide tool," *Tribology International*, vol. 42, no. 0301-679X, pp. 738-744.

[26] Astakhov, V.P., 1999,*Metal Cutting Mechanics*. Boca Raton: CRP Press.

[27] V.P. Astakhov, 2011,"Authentication of FEM in Metal Cutting," in *Finite Element Method in Manufacturing Processes*, J.P. Davim, Ed.: Willey, pp. 1-43.

[28] Duan, C.Z., Dou, T., and Wang, M., 2010,"Research on Influence of Material Hardness and Cutting Conditions on Serrated Chip Formation Process during High Speed Machining of AISI 1045 Hardened Steel," in *Computer Engineering and Technology (ICCET), 2nd International Conference*, Chengdu, pp. 552-555.

[29] Astakhov, V.P. and Xiao, X., 2008,"A methodology for practical cutting force evaluation based on the energy spent in the cutting system," *Machining Science and Technology*, vol. 12, pp. 325-347.

[30] Astakhov, V.P., 2010,*Geometry of Single-point Turning Tools and Drills: Fundamentals and Practical Applications*. London: Spriger.

[31] Jawahir, I.S. and Zhang, J.P., 1995,"An analysis of chip curl development, chip deformation and chip breaking in orthogonal machining," *Transactions-North American Manufacturing Research Institution of SME*, pp. 109-114.

